LBNL-45435
Preprint

ERNEST ORLANDO LAWRENCE
BERKELEY NATIONAL LABORATORY

Primary and Secondary Processes in the Photodissociation of $CHBr_3$

W. Sean McGivern, Osman Sorkhabi, Arthur G. Suits,
Agnes Derecskei-Kovacs, and Simon W. North

Chemical Sciences Division

March 2000

Submitted to
Journal of Physical Chemistry

REFERENCE COPY
Does Not
Circulate
Bldg. 50 Library - Ref.
Lawrence Berkeley National Laboratory

LBNL-45435
Copy 1

DISCLAIMER

This document was prepared as an account of work sponsored by the United States Government. While this document is believed to contain correct information, neither the United States Government nor any agency thereof, nor the Regents of the University of California, nor any of their employees, makes any warranty, express or implied, or assumes any legal responsibility for the accuracy, completeness, or usefulness of any information, apparatus, product, or process disclosed, or represents that its use would not infringe privately owned rights. Reference herein to any specific commercial product, process, or service by its trade name, trademark, manufacturer, or otherwise, does not necessarily constitute or imply its endorsement, recommendation, or favoring by the United States Government or any agency thereof, or the Regents of the University of California. The views and opinions of authors expressed herein do not necessarily state or reflect those of the United States Government or any agency thereof or the Regents of the University of California.

LBNL-45435

Primary and Secondary Processes in the Photodissociation of $CHBr_3$

W. Sean McGivern,[a] Osman Sorkhabi,[b] Arthur G. Suits,[b]
Agnes Derecskei-Kovacs,[a] and Simon W. North[a]

[a]Department of Chemistry
Texas A&M University
College Station, Texas 77842

[b]Department of Chemistry
University of California, Berkeley
and
Chemical Sciences Division
Ernest Orlando Lawrence Berkeley National Laboratory
University of California
Berkeley, California 94720

March 2000

This work was supported by the Director, Office of Science, Office of Basic Energy Sciences, Division of Chemical Sciences, of the U.S. Department of Energy under Contract No. DE-AC03-76SF00098.

Primary and Secondary Processes in the Photodissociation of $CHBr_3$

W. Sean McGivern[a], Osman Sorkhabi[b], Arthur G. Suits[b] , Agnes Derecskei-Kovacs[a], and Simon W. North[a]

[a]*Department of Chemistry, Texas A&M University, College Station TX 77842; and* [b]*Chemical Sciences Division, Lawrence Berkeley Laboratory, University of California, and Chemistry Department, University of California, Berkeley, CA, 94720*

Abstract

The photodissociation of $CHBr_3$ at 193 nm has been investigated using photofragment translational spectroscopy with VUV ionization detection. The only primary process observed was the loss of bromine atom. The translational energy distribution for this channel suggests a direct dissociation from an excited electronic state, and the anisotropy parameter, β=0.0, is consistent with a transition dipole moment aligned perpendicular to C_{3v} axis. The majority of nascent $CHBr_2$ fragments undergo secondary dissociation *via* two competing channels. The elimination of HBr and C-Br bond cleavage in $CHBr_2$ occur with comparable yields. We also provide *ab initio* calculations on the relevant photochemical species and RRKM estimates of the product branching ratios that are consistent with the experimental observations.

Submitted to *J. Phys. Chem.*, January 25, 2000 1 Table, 9 Figures
Revisions submitted: March 29, 2000

Proofs to: Simon W. North
Department of Chemistry
Texas A&M University
P.O. Box 300012
College Station, TX 77842

e-mail: north@mail.chem.tamu.edu.

I. INTRODUCTION

The role of anthropogenic and natural sources of chlorine-containing molecules in stratospheric ozone depletion has been well established.[1] The influence of bromine and its chemistry on the atmosphere, however, has received considerably less attention. Bromine in the stratosphere depletes ozone *via* a chain reaction mechanism analogous to the well-known ClO_x cycle,

$$Br + O_3 \rightarrow BrO + O_2$$
$$BrO + O \rightarrow Br + O_2$$

Although the concentration of bromine in the stratosphere is much lower than chlorine, the reservoir species which temporarily confine reactive bromine are photochemically labile and, therefore, inefficient. As a result, bromine is far more destructive to stratospheric ozone than chlorine on an atom for atom basis.[2] Recent estimates by Garcia and Solomon report that this factor could be as high as 100, suggesting that bromine may be as important in stratospheric ozone depletion as chlorine.[3] In addition to catalytic bromine cycles, the coupling of BrO and ClO cycles to produce free bromine and chlorine atoms *via* the reaction,

$$BrO + ClO \rightarrow Br + Cl + O_2$$

can enhance the depletion of ozone by chlorofluorocarbons by up to 20 percent for even moderate mixing ratios of bromine in the stratosphere. Despite the influence of the solar ultraviolet photolysis that both bromine sources and reservoir species have on the reactive bromine budget of the atmosphere, there is a severe lack of experimental data regarding the photodissociation of these molecules.

Bromoform is one of several volatile halocarbon compounds that contribute active bromine to the atmosphere. It is primarily of biogenic origin and is produced in the Arctic by both kelp and ice algae as a byproduct of photosynthetic processes.[4] Other natural sources include emissions from oceanic microalgae that result in large concentrations of bromocarbons in the marine boundary layer.[5] Of the bromomethane derivatives, bromoform has been found to be the greatest contributor of bromine to the Arctic atmosphere[6] with an atmospheric lifetime of approximately two weeks.[7] Despite its importance, relatively few studies of its photochemistry have been performed. At

wavelengths near 200 nm there are several energetically accessible dissociation pathways, including both two-body and three-body processes,

$$CHBr_3 \rightarrow CHBr_2 + Br(^2P_J) \qquad (J = 1/2, 3/2) \qquad [1]$$
$$\rightarrow CHBr + Br_2 \qquad [2]$$
$$\rightarrow CBr_3 + H \qquad [3]$$
$$\rightarrow CBr_2 + HBr \qquad [4]$$
$$\rightarrow CBr + HBr + Br \qquad [5]$$
$$\rightarrow CHBr + Br + Br \qquad [6]$$

Simons and Yarwood have studied the photodissociation of $CHBr_3$ using flash photolysis near 200 nm.[8] Spectral features corresponding to vibronic transitions associated with CBr were observed following photolysis. The authors asserted that the origins of CBr involved the primary loss of bromine atom followed by the spontaneous decomposition of the energized $CHBr_2$ radical. Power dependence studies indicated that the CBr was the result of a single photon process. Stern-Volmer experiments varying buffer gas pressures at several different excitation energies and RRK calculations provided information on the threshold for CBr formation from $CHBr_2$. Sears and co-workers have subsequently used $CHBr_3$ phototolysis at 193 nm as a means to prepare CBr for infrared spectroscopic studies.[9] The authors were also able to obtain the CHBr radical from $CHBr_3$ at this wavelength and determined that the products also resulted from a single photon process, suggesting an additional fate of the energized $CHBr_2$ radicals.[10,11]

In the present paper we have examined the photodissociation of $CHBr_3$ at 193 nm. We find that the dissociation involves both primary and secondary fragmentation channels resulting in bromine atom quantum yields greater than unity and the release of HBr. The primary step in the dissociation is the rapid loss of atomic bromine resulting in a $CHBr_2$ radical with sufficient internal energy to dissociate *via* the loss of Br and HBr with comparable yields. The use of VUV ionization as opposed to electron impact for product detection is ideally suited for studying complex multichannel dissociation processes, where excessive dissociative ionization can significantly complicate the analysis. Analysis of such data, in addition to RRKM calculations using *ab initio* energies and geometries, permits a precise determination of the photofragment quantum yields and

provides valuable thermodynamic information, including the barrier height for HBr elimination from $CHBr_2$.

II. EXPERIMENTAL

The fixed detector-rotating source molecular beam apparatus has been described in detail previously.[12] A continuous molecular beam of <1% bromoform seeded in helium was collimated with conical skimmers and intersected at 90° with the output of a Lambda Physik LPX-200 excimer laser operating on the ArF transition (193 nm). There was no change in the shape of any of the TOF spectra over a laser fluence range of 60-500 mJ/cm^2 providing strong evidence that all of the observed signals are the result of single photon absorption. Neutral photodissociation products traveled 15.1 cm where they were ionized by tunable VUV undulator radiation, mass selected, and counted as a function of time. The characteristics of the VUV undulator radiation used for product photoionization have also been previously described.[13] The nozzle was heated to 100°C to minimize clustering in the beam and no evidence for clusters was observed. A pile-of-plates polarizer, consisting of 8 quartz plates at Brewster's angle, was used to polarize the excimer beam, resulting in >85% linear polarization. Rotation of the linear polarized beam was achieved using a half-wave plate (Karl Lambrecht).

Bromoform 99% was obtained from Aldrich Chemical Co. and used without further purification.

III. RESULTS AND ANALYSIS

Center-of-mass translational energy, $P(E_T)$, distributions were obtained from the time of flight (TOF) spectra using the forward convolution technique.[14] For all of the TOF spectra presented, the circles represent the data and the lines represent the forward convolution fit.

TOF spectra were obtained for several masses: $CHBr^+$ (m/z 92), Br^+ (m/z 79, 81), HBr^+ (m/z 80 82), and CBr^+ (m/z 91). No signal was observed for $CHBr_2^+$ (m/z 173) at VUV ionization energies from 15 eV to 8 eV. Although the ionization energy for $CHBr_2$ is 8.13 eV[15] it is formed with an average internal energy (*vide infra*) which exceeds the threshold for $CHBr^+$ upon ionization above threshold.[16] As a result this species only

contributes to the m/z 92 ($CHBr^+$) TOF spectra. The ionization energy dependence of both Br^+ and HBr^+ signals showed no change in shape as the energy was varied from 15 eV to 12 eV, indicating that there is no contribution from dissociative ionization to these TOF spectra. No CBr_2^+ was detected (ionization energy of 10.1 eV), and no evidence of this fragment at lower masses was observed.

A. Primary Dissociation and Product Identification

TOF spectra for m/z 92 ($CHBr^+$) at laboratory angles of 10°, 15° and 20° are shown in Figure 1. There are two contributions to the CHBr spectra. The first contribution, indicated by the solid line, results from the dissociative ionization of $CHBr_2$ fragments. The second contribution (dashed line) is from CHBr fragments that arise from the spontaneous dissociation of $CHBr_2$. Figure 2 shows the ionization dependence of the CHBr TOF spectra which confirms the identity of the contributions. As the VUV energy is decreased to 11 eV the contribution attributed to $CHBr_2$ daughter fragments shows a significant decrease relative to the CHBr fragments. The ionization energy of CHBr is 8.94 eV[17] and signals associated with this fragment persist near threshold although the overall signal is greatly reduced. Figure 3 shows Br^+ (m/z 79) TOF spectra at laboratory angles of 15° and 30° and a photoionization energy of 15 eV. There are also two contributions to the m/z 79 spectra; a fast contribution near the leading edge of the profile (solid line) and a contribution at longer times (dashed line). The fast component can be attributed to primary loss of Br from $CHBr_3$ and has been fitted using the $P(E_T)$ distribution shown in the top panel of Figure 4. The $P(E_T)$ distribution is nearly Gaussian in shape with a maximum at 13 kcal/mol and a FWHM of 8 kcal/mol. The $CHBr_2$ internal energy corresponding to the total translational energy is indicated on the top axis, assuming that the bromine atom is formed in its ground spin-orbit state, $Br(^2P_{3/2})$. Only the fastest Br signal can be momentum-matched to the features assigned to $CHBr_2$ fragments in Figure 1. The $P(E_T)$ distribution used to fit the primary $CHBr_2$ is shown in the bottom panel of the figure corresponding to a threshold for secondary dissociation near 68 kcal/mol.[18] The fits to the m/z 92 TOF spectra are extremely sensitive to changes in the leading edge of the $CHBr_2$ $P(E_T)$ distribution, providing a good estimate of the threshold energy. Although HBr fragments are detected, they cannot be attributed to a

primary dissociation channel. Therefore, we find that the only observed primary channel is the loss of bromine atom and the remaining products are the result of secondary processes.

Photofragment angular distributions were recorded as a function of laser polarization using the leading edges of the Br^+ and $CHBr^+$ signals at a laboratory angle of 10°. The laboratory angular distributions, $I(\theta)$ are,

$$I(\theta) = \frac{1}{4\pi}\left[1 + \beta P_2(\cos\theta)\right]$$

where β is the anisotropy parameter and $P_2(x)$ is the second Legendre polynomial. For prompt dissociation in the axial recoil limit the anisotropy parameter is given by $\beta = 2P_2(\cos\chi)$ where χ is the angle between the recoil velocity vector and the transition dipole moment. No polarization dependence was observed for either mass, corresponding to an anisotropy parameter of $\beta = 0.0 \pm 0.1$.

B. Secondary Dissociation of the $CHBr_2$ Radical

The lack of momentum matching between the Br and $CHBr_2$ fragments is strong evidence for secondary dissociation. Only the Br loss channel (5) and the HBr elimination channel (6) are energetically accessible at 193 nm, and we see evidence for both channels in the TOF spectra. The forward convolution fitting of secondary dissociation processes has been discussed in detail previously.[19,20] A primary $P(E_T)$ distribution is first chosen to represent the translational energy of those primary fragments which undergo secondary decomposition. In principle, this can be determined by subtracting the $P(E_T)$ distribution derived from fitting the $CHBr_2$ fragment from the $P(E_T)$ distribution for the Br fragment. There are two secondary channels, however, each with a different energetic threshold. As a consequence the leading edge of the distribution in the lower panel of figure 4 corresponds only to the lowest threshold process. We have relied on *ab initio* and RRKM calculations to provide additional information for assigning these thresholds. We find that the threshold for HBr loss is lower in energy (68.0 kcal/mol) than for Br elimination (73.6 kcal/mol), and therefore the abrupt truncation point in the $CHBr_2$ $P(E_T)$ distribution corresponds to the onset of HBr loss. Based on RRKM calculations, discussed in detail below, once the Br loss channel is

energetically accessible, it becomes the dominant dissociation pathway for $CHBr_2$. Therefore, primary $CHBr_2$ fragments with internal energy greater than the HBr loss threshold but less than the Br loss threshold contribute to channel 5 while the $CHBr_2$ fragments with internal energy greater than the Br loss threshold contribute only to channel 6. The resulting primary $P(E_T)$ distributions for each secondary channel are shown in Figure 5 and provide very good fits to the data. It should be noted that initial attempts to iteratively fit the data without the *ab initio* constraints resulted in quantitatively similar distributions providing additional support for the locations of the secondary thresholds.

The secondary dissociation lifetimes for both channels were assumed to exceed the rotational period resulting in a forward-backward symmetric secondary angular distribution.[21,22] Fits to the TOF spectra for each secondary channel were obtained by iteratively adjusting the secondary angular distribution, maintaining forward-backward symmetry, and the secondary $P(E_T)$ distribution. Fragments associated with the Br loss channel appear as the central feature in the $CHBr^+$ spectra and the slow feature in the Br^+ spectra. The best fit secondary $P(E_T)$ distribution for this channel is shown in the top panel of Figure 7. Fragments arising from the HBr elimination channel represent the sole contributions to the HBr^+ and CBr^+ TOF spectra shown in Figure 6. The secondary $P(E_T)$ for the HBr loss channel is shown as the bottom panel in Figure 7. Both distributions peak at low translational energies suggesting almost no barrier to recombination. On average there is little energy available (<19 kcal/mol) for the fragments of secondary dissociation. The sensitivity of the fits to the secondary $P(E_T)$ distributions is modest and depends on the choice of each corresponding primary $P(E_T)$. However, the qualitative result that both are peaked near zero is robust.

IV. DISCUSSION

A. Primary Dissociation Mechanism

The measured isotropic spatial distribution of the photofragments could be the result of several factors. If the dissociation is not prompt on the time-scale of parent rotation,

the correlation between the direction of the electric dipole moment and the relative velocity will be diminished by parent rotation. Based on previous work on halogenated methane derivatives[23] and the observed translational energy distribution, however, we believe that the primary dissociation is direct, involving excitation to a repulsive state. The impulsive model, which provides an adequate description of direct dissociation, predicts an average translational energy of 16 kcal/mol in reasonable agreement with the measured value. A fast dissociation can also produce an isotropic velocity distribution if the angle between the recoil direction and the transition dipole moment, χ, is 54.7°. In C_{3v} symmetry an $A_1 \leftarrow A_1$ transition requires that the transition dipole moment lies along the three-fold axis and gives χ=72.7° resulting in an anisotropy parameter of β=-0.73, based on an *ab initio* geometry optimization of $CHBr_3$. The dipole moment for an $E \leftarrow A_1$ transition is perpendicular to this axis and yields β=-0.05 after averaging over the azimuthal orientation of the bromine atoms. This result is consistent with our observations.

Although there is no direct experimental evidence, we do not expect that spin-orbit excited bromine, $Br(^2P_{1/2})$, is formed in significant yield. The truncation of the primary $P(E_T)$ distribution required to fit the $CHBr_2$ contribution shown in Figure 1 is very abrupt. The formation of substantial excited state bromine would result in stable $CHBr_2$ with translational energies approaching zero which is not observed. In addition, the quantum yields for primary and secondary Br are more consistent with the absence of excited Br. We are unable, however, to rule out a minor contribution of excited state bromine. State-selected experiments could provide a definitive determination of the spin-orbit branching in the dissociation.

B. Ab initio and RRKM Calculations on the dissociation of CHBr2

In order to understand more about the photodissociation of $CHBr_3$, and in particular, the competition between secondary dissociation channels, we have performed *ab initio* and RRKM calculations. All *ab initio* calculations were performed using Gaussian 94[24] on an Origin 2000 Supercomputer and an SGI Power Challenge workstation. Geometries and frequencies for the ground state species were calculated at the MP2/6-311+G* level, and vibrational frequencies were left unscaled for the zero-point

corrections and RRKM calculations. The transition state for the HBr loss channel was optimized at the MP2/6-31+G* level, and single-point energies were calculated at the MP2/cc-pVtz level. Relevant geometries for the secondary dissociation products and transition state are shown in Figure 9. Recently, a methodology has been developed to correct carbon-halogen bond energies for basis set effects beyond the triple-zeta level and correlation effects beyond the MP2 approximation by applying corrections to MP2/cc-pVtz energies.[25] Using this methodology, we have calculated final zero-point corrected C-Br bond energies of 63.8 kcal/mol and 73.6 kcal/mol for $CHBr_3$ and $CHBr_2$ respectively. The former value was calculated previously[25] and is in good agreement with previous theoretical[26] (62.7 ± 0.9 kcal/mol) and experimental[27] (66 ± 4 kcal/mol) results. The HBr loss channel is endothermic with a reaction energy of 67.4 kcal/mol, very close to previous reports[28], and a barrier height of 68.0 kcal/mol. Calculated energies are shown schematically in Figure 8. The very small exit barrier from the three-center elimination of HBr is consistent with previous reports of three-center hydrogen halide elimination. Riehl and Morokuma have examined the three-center elimination of HCl from vinyl chloride.[29] The calculated transition state is qualitatively similar to the HBr transition state of the present study with an elongated carbon-halogen bond length and a modestly lengthened C-H bond (Figure 9). The exit barrier for HCl loss was calculated to be only 2.6 kcal/mol above the asymptotic products. In the present study, the HBr loss channel from $CHBr_2$ is found to be only 0.6 kcal/mol higher than the asymptotic product energy. The smaller barrier found for $CHBr_2$ is not surprising given that bromine atom can interact with the hydrogen more readily in the present system due to its larger size and relative proximity to the reacting hydrogen in a tetrahedral geometry.

Microcanonical unimolecular rates, $k(E,J)$, have been evaluated using and RRKM and variational RRKM calculations[30] to describe the HBr and Br loss channels respectively. For consistency all frequencies and energies used in the RRKM calculations, including reactant and product species, were obtained from *ab initio* theory. A direct count algorithm was used to determine the sum of states using the harmonic oscillator approximation for both sets of calculations. The rate of HBr loss was calculated using the optimized *ab initio* transition state geometries and frequencies.

The unimolecular rates for the Br elimination channel were performed using variational RRKM theory,[30] minimizing the sum of states along the reaction coordinate,

$$\frac{dN^{\ddagger}(E,J,R^{\ddagger})}{dR} = 0.$$

The frequencies of the transitional modes were assumed to change smoothly according to

$$\nu_i(R) = \nu_i(R_e)\exp(-aR),$$

where R_e is the equilibrium C-Br bond length, and a is a constant taken to be 1.2.[31,32] The sum of a Morse function and a centrifugal barrier was used to model the potential along the C-Br stretching coordinate. The centrifugal barrier was derived using the average rotational energy of the $CHBr_2$ corresponding to $J = 111$ derived from the soft fragment impulsive model[33] following primary loss of bromine. Moments of inertia at each fixed geometry were obtained by changing only the C-Br bond length. One rocking mode and one wagging mode were treated as transitional modes. The remaining modes were assumed to be well-represented by the product frequencies.

RRKM and variational RRKM calculations were performed at a series of energies above the respective threshold energies for HBr and Br channels corresponding to the measured $CHBr_2$ internal energy distribution. Table 1 summarizes the results as a function of the internal energy of the $CHBr_2$ fragment after the initial Br loss from $CHBr_3$. Rates for Br loss increase from 1×10^{12} s^{-1} to 2×10^{13} s^{-1} for energies above threshold up to 10 kcal/mol. Rates for HBr elimination range from 1.5×10^{9} s^{-1} near threshold to 7×10^{11} s^{-1} at the maximum energies available. Clearly for $CHBr_2$ internal energies above the threshold for Br loss, the rate of Br loss exceeds the rate for HBr elimination by more than an order of magnitude. As a result, $CHBr_2$ fragments with internal energies above 73.6 kcal/mol will predominately form CHBr + Br. The collision frequency at ambient tropospheric conditions at 300 K is on the order of 10^{9} s^{-1} suggesting that $CHBr_2$ radicals with internal energies above the Br threshold will not be collisionally stabilized. However, $CHBr_2$ fragments with internal energies near the HBr elimination threshold may be quenched prior to reaction. This is consistent with the work of Simons and Yarwood[8], who observed pressure dependent-quantum yields for the CBr products in $CHBr_3$ dissociation near 200 nm. Given that the peak of the $P(E_T)$ distribution for $CHBr_2$ is near this threshold, a significant fraction of $CHBr_2$ fragments would be

expected to be stabilized in the atmosphere in contrast to the collisionless conditions present in a molecular beam experiment.

C. Product Branching Ratios

We can estimate the branching ratio for the secondary dissociation channels and obtain Br and HBr quantum yields based on the primary $P(E_T)$ distributions used to fit the TOF spectra. Assuming that the quantum yield for the primary bromine atoms is unity, the quantum yields for secondary Br and HBr can be determined by integrating the normalized $P(E_T)$ distribution in the top panel of Figure 4 over the limits illustrated in Figure 5 for each secondary channel. This analysis gives quantum yields for the secondary Br and HBr channels of 0.3 and 0.4 respectively. Therefore, the total yield for bromine atoms is 1.3 using this procedure. A quantum yield for Br atoms based on the relative contributions of primary and secondary channels to the Br TOF spectra is consistent with this value, although slightly higher value is obtained than from the $P(E_T)$ distributions. The observation of bound $CHBr_2$ in the m/z 92 ($CHBr^+$) TOF spectra and the location of the lower threshold to secondary dissociation provides an upper limit of 1.7 to the Br quantum yield. Since Br loss *via* a barrierless dissociation from $CHBr_2$ dominates HBr elimination above threshold and significant secondary HBr is observed, it is unlikely that the Br quantum yield is close to this upper bound. We, therefore, assign a quantum yield of 1.5±0.2, which reflects the upper and lower bounds of analysis. Accordingly we assign a final HBr quantum yield of 0.2±0.2.

Based on our calculated thresholds we can also comment on the wavelength dependence on the Br quantum yield. At wavelengths longer than 209 nm there is insufficient energy for the formation of secondary Br and the Br quantum yield should be unity. Above 218 nm there is insufficient energy for the secondary dissociation of $CHBr_2$ towards HBr elimination and only primary C-Br bond cleavage will occur. Of course, the precise quantum yields of Br and HBr at wavelengths shorter than these limits will depend intimately on the partitioning of the available in the primary dissociation step and will be more difficult to predict *a priori*. We note that Br loss from $CHBr_2$ should become increasingly dominant over HBr loss as the internal energy of the $CHBr_2$ radicals increases.

IV. CONCLUSIONS

The photodissociation of $CHBr_3$ has been investigated at 193 nm using photofragment translational spectroscopy with VUV ionization for product detection. We have identified and characterized both primary and secondary dissociation channels in the dissociation. The primary dissociation involves prompt C-Br bond fission. A fraction of the $CHBr_2$ radicals formed in the primary step contain sufficient energy to undergo spontaneous secondary dissociation *via* the elimination of both HBr and Br to a comparable extent. *Ab initio* calculations have provided important thermochemical information on the fragmentation of $CHBr_2$ including the transition state associated with HBr elimination. RRKM calculations have shown that significant secondary HBr may be formed in addition to secondary bromine fragments; however, under ambient tropospheric conditions, $CHBr_2$ fragments with internal energies below the Br-loss threshold may be collisionally stabilized prior to reaction.

V. ACKNOWLEDGMENTS

Work by SWN and WSM was partially supported by a Research Enhancement from Texas A&M University. The work by AGS and OS was supported by the Director, Office of Energy Research, Office of Basic Energy Science, Chemical Sciences Division of the U. S. Department of Energy under contract No. DE-AC03-76SF00098. The experiments were conducted at the Advanced Light Source, Lawrence Berkeley National Laboratory which is supported by the same source. Hardware and software support for the *ab initio* calculations was given by the Texas A&M University Supercomputing Facility and Texas A&M University Laboratory for Molecular Simulations under National Science Foundation grant CHE-9528196.

Figure Captions:

Figure 1: Unpolarized TOF spectra for m/e 92 ($CHBr^+$) photoproducts at a scattering angle of 10°, 15°, and 20° and a photoionization energy of 15.0 eV. The circles are the experimental data, and the solid lines are the forward convolution fits using the $P(E_T)$ distributions in figure 4.

Figure 2: Experimental TOF spectra for m/e 92 ($CHBr^+$) at 15° and a photoionization energy of 15.0 eV (top trace) and 8 eV (bottom trace).

Figure 3: Unpolarized TOF spectra for m/e 79 (Br^+) at scattering angles of 15° and 30° and a photoionization energy of 15.0 eV. The circles are the experimental data, the solid line is the forward convolution fit using the $P(E_T)$ distribution shown in top panel of figure 4, and the dashed line is the contribution from secondary Br loss from the $CHBr_2$ radical.

Figure 4: The upper panel shows the primary $P(E_T)$ used to fit the fastest Br contribution in the TOF spectra in figure 3. The internal energy of the $CHBr_2$ radical, formed in coincidence with ground state bromine, is indicated on the top axis. The lower panel shows the primary $P(E_T)$ distribution used to fit the $CHBr_2$ contribution to the m/z 92 TOF spectra in figure 1.

Figure 5: The upper panel shows the primary $P(E_T)$ distribution used to model the secondary Br loss from $CHBr_2$. The lower panel shows the primary $P(E_T)$ distribution used to model the HBr elimination from $CHBr_2$. The thresholds for secondary Br and HBr loss are indicated by the arrows in the upper panel.

Figure 6: The upper panel shows the secondary $P(E_T)$ distribution corresponding to the Br loss from the $CHBr_2$ radical. The lower panel shows the secondary $P(E_T)$ distribution for HBr elimination from $CHBr_2$.

Figure 7: Experimental TOF spectra for m/e 91 (CBr^+) at 15° (upper panel) and for m/e 82 (HBr^+) at 20° (lower panel) for a photoionization energy of 15.0 eV. The circles are the experimental data and the solid lines are the forward convolution fits to the data using the primary $P(E_T)$ distribution in the lower panel of figure 5 and the secondary $P(E_T)$ distribution in the lower panel of figure 6.

Figure 8: Schematic energy diagrams for the secondary dissociation of the $CHBr_2$ radical. The energies are the result of *ab initio* calculations as described in the text.

Figure 9: Optimized geometries of $CHBr_2$, CHBr, CBr, and the transition state for the HBr loss channel. Lengths are in Angstroms, and angles are in degrees. The $CHBr_2$ radical shows a slight nonplanarity with an angle of 33.0° between the two HCBr planes.

Table 1: RRKM and var-RRKM microcanonical rates for the dissociation of $CHBr_2$

E^* (kcal/mol)	E_T (kcal/mol)[a]	$k(CHBr_2 \rightarrow CBr + HBr)$ [s^{-1}]	$k(CHBr_2 \rightarrow CHBr + Br)$ [s^{-1}]
84	0.2	6.95×10^{11}	1.94×10^{13}
83	1.2	5.70×10^{11}	1.56×10^{13}
81	3.2	3.69×10^{11}	1.02×10^{13}
79	5.2	2.24×10^{11}	6.01×10^{12}
77	7.2	1.25×10^{11}	3.01×10^{12}
75	9.2	6.18×10^{10}	1.26×10^{12}
73	11.2	2.59×10^{10}	-
71	13.2	8.25×10^{9}	-
69	15.2	1.47×10^{9}	-

[a]Total translational energy for the $CHBr_2$ and Br fragments following 193 nm photodissociation of $CHBr_3$.

References

[1] Molina, M. J.; Rowland, F.S. *Nature*, **1974**, *248*, 810.

[2] Solomon, S.; Mills, M.; Heidt, L. E.; Pollock, W. H.; Tuck, A.F. *J. Geophys Res.* **1992**, *97*, 25. S. Solomon M.

[3] Garcia, R. R.; Solomon, S. *J. Geophys. Res.* **1994**, *99*, 12937.

[4] Cota, G. F; Sturges, W.J. *Mar. Chem.* **1997**, *6*, 181.

[5]Class,T.; Kohnle, R.;Ballschmiter, K. *Chemosphere* **1986,** *15*, 429.

[6] Itoh, N.; Shinya, M. *Mar. Chem.* **1994**, *45*, 95.

[7] Barrie, L.A.; Bottenheim, J.W.; Schnell, R.C.; Crutzen, P.J. Rasmussen, R.A. *Science* **1988**, *334*, 138.

[8] Simons, J. P.; Yarwood, A. J. *Trans Faraday Soc.* **1961**, *57*, 2167.

[9] Marr, A. J.; Sears, T. J.; Davies, P.B. *J. Mol. Spectrosc.* **1997**, *184*, 413.

[10] Chang, B.-C.; Sears, T. J. *J. Chem. Phys.* **1996**, *105*, 2135.

[11] Marr, A. J.; North, S. W.; Sears, T.J.; Ruslen, L.; Field, R. W. *J. Mol. Spectrosc.* **1998**, *188*, 68.

[12] Yang, X.; Blank, D. A.; Lin, J.; Heimann, P. A.; Wodtke, A. M.; Suits, A.; Lee, Y. T. *Rev. Sci. Instrum.* **1997**, *68*, 3317.

[13] Koike, M.; Heimann, P. A.; Kung, A. H.; Namioka, T.; DiGennaro, R.; Gee, B.; Yu, N. *Nuclear Instruments and Methods in Physics Research* **1994**, *347*, 282.; Heimann, P. A.; Koike, M.; Hsu, C. W.; Evans, M.; Ng, C. Y.; Blank, D.; Yang, X. M.; Flaim, C.; Suits, A. G.; Lee, Y. T. *SPIE Proceedings* 1996, p. 2865.

[14] Zhao, X. Ph.D. Thesis, University of California, Berkeley, 1989.

[15] Andrews, L.; Dyke, J. M.; Jonathan, N.; Keddar, N.; Morris, A. *J. Phys. Chem.* **1984**, *88*, 1950.

[16] The $CHBr_2^+$ is observed as daughter fragment of $CHBr_3$ in on axis TOF measurements to determine the velocity distribution of the molecular beam.

[17]Li, Z.; Francisco, J. S. *J. Chem. Phys.* **1998**, *109*, 134.

[18] For a discussion on obtaining thresholds for secondary processes based on this approach see North, S. W.; Blank, D. A.; Lee, Y. T. *Chem. Phys. Lett.* **1994**, *224*, 38;

Blank, D. A.; North, S. W.; Stranges, D.; Suits, A. G.; Lee, Y. T.; *J. Chem. Phys.* **1997**, *106*, 539.

[19] Wodtke, A. M. Ph.D. Thesis, University of California, Berkeley, 1986; Zhao, X. Ph.D. Thesis, University of California, Berkeley, 1989.

[20] Zhao, X.; Nathanson, G. M.; Lee, Y. T. *Acta Physico-Chim. Sinica* **1992**, *8*, 70.

[21] North, S. W.; Blank, D. A.; Lee, Y. T.; *Chem. Phys. Lett.* **1994**, *224*, 38; Kroger, P. M.; Riley, S. J. *J. Chem. Phys.* **1977**, *67*, 4483.

[22] Hinsta, E. J.; Zhao, X.; Lee, Y. T. *J. Chem. Phys.* **1990**, *92*, 2280.

[23] Sparks, R. K.; Shobatake, K.; Carlson, L .R.; Lee, Y. T. *J. Chem. Phys.* **1981**, *75*, 3838; Gougousi, T.; Samartzis, P. C.; Kitsopolous, T. N. *J. Chem. Phys.* **1998**, *108*, 5742; McGivern, W. S.; Li,; Zou, P.; North, S. W. *J. Chem. Phys.* **1999**, *111*, 5771.

[24] Frisch, M. J.; Trucks, G. W.; Schlegel, H. B.; Gill, P. M. W.; Petersson, G. A.; Montgomery, J. A.; Raghavachari, K.; Al-Laham, M. A.; Zakrzewski, V. G.; Ortiz, J. V.; Foresman, J. B.; Cioslowski, J.; Stefanov, B. B.; Nanayakkara, A.; Challacombe, M.; Peng, C. Y.; Ayala, P. Y.; Chen, W.; Wong, M. W.; Andres, J. L.; Replogle, E. S.; Gomperts, R.; Martin, R. L; Fox, D. J.; Binkley, J. S.; Defrees, D. J.; Baker, J.; Stewart, J. P.; Head-Gordon, M.; Gonzalez, C.; Pople, J. A. GAUSSIAN 94, Revision D.4, Gaussian, Inc., Pittsburgh PA, 1995.

[25] McGivern, W. S.; Derecskei-Kovacs, A.; North, S. W.; Francisco, J. F. *J. Phys. Chem. A* **2000**, *104*, 436.

[26] Paddison S. J.; Tschuikow-Roux, E. *J. Phys. Chem.* **1998**, *102*, 6191.

[27] Miller, W. J.; Palmer, H. B. *J. Chem. Phys.* **1964**, *40*, 3701.

[28] The enthalpy of reaction for the reaction $CHBr_2 \rightarrow CBr + HBr$ can be determined to be 65.2 kcal/mol based on a recent estimate for the heat of formation for $CHBr_2$ of 48.1kcal/mol in Ref 26.

[29] Riehl, J-F; Morokuma, K. *J. Chem. Phys.* **1994**, *100*, 8976.

[30] Holbrook, K. A.; Pilling, M. J.; Robertson, S. H. *Unimolecular Reactions*, 2nd Ed; Wiley Interscience: New York, 1996; Forst, W. *Theory of Unimolecular Reactions*; Academic Press: New York, 1973.

[31] Hase, W. L. *Chem. Phys. Lett.* **139**, 389 (1987).

[32] Sudbo, A. S.; Schultz, P. A.; Grant, E. R.; Shen, Y. R.; Lee, Y. T. *J. Chem. Phys.* **70**, 921 (1979).

[33] Busch, G. E.; Wilson, K. R. *J. Chem. Phys.* **1972**, *56*, 3639.

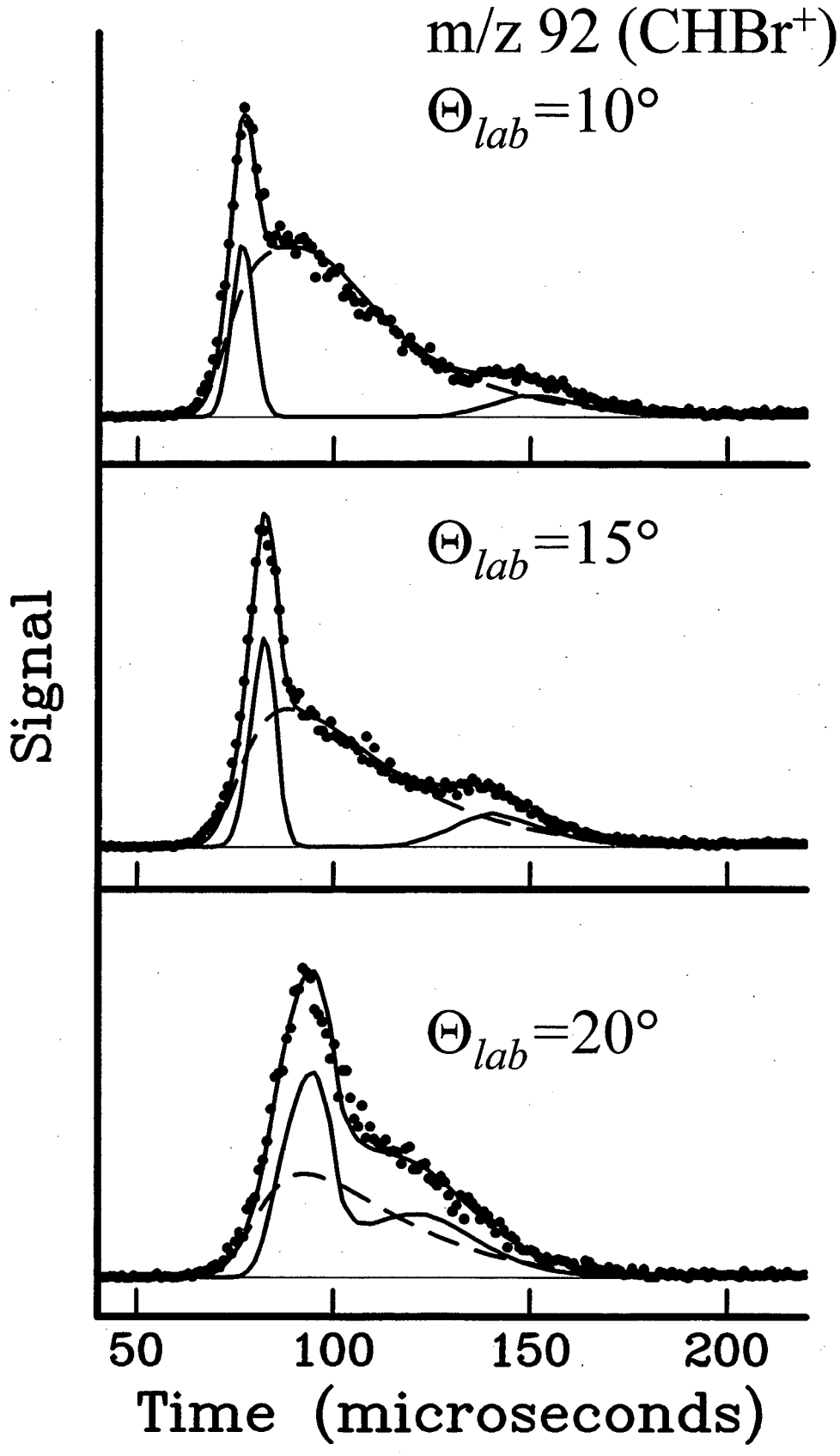
m/z 92 (CHBr+)
Θlab=10°
Θlab=15°
Θlab=20°
Signal
50
100
150
200
Time (microseconds)

Fig 1

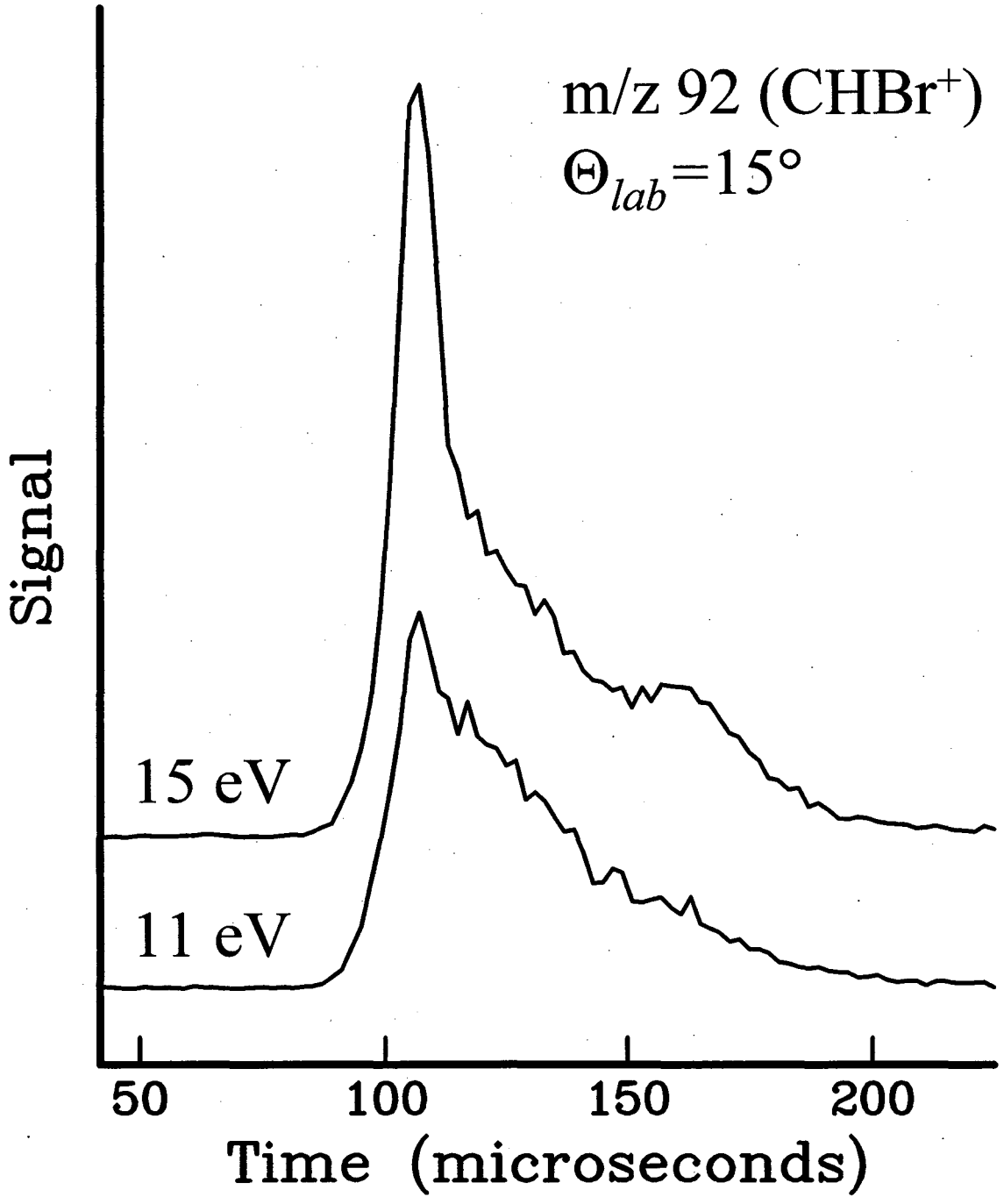
m/z 92 (CHBr+)
Θlab=15°
Signal
15 eV
11 eV
50
100
150
200
Time (microseconds)

Fig 2

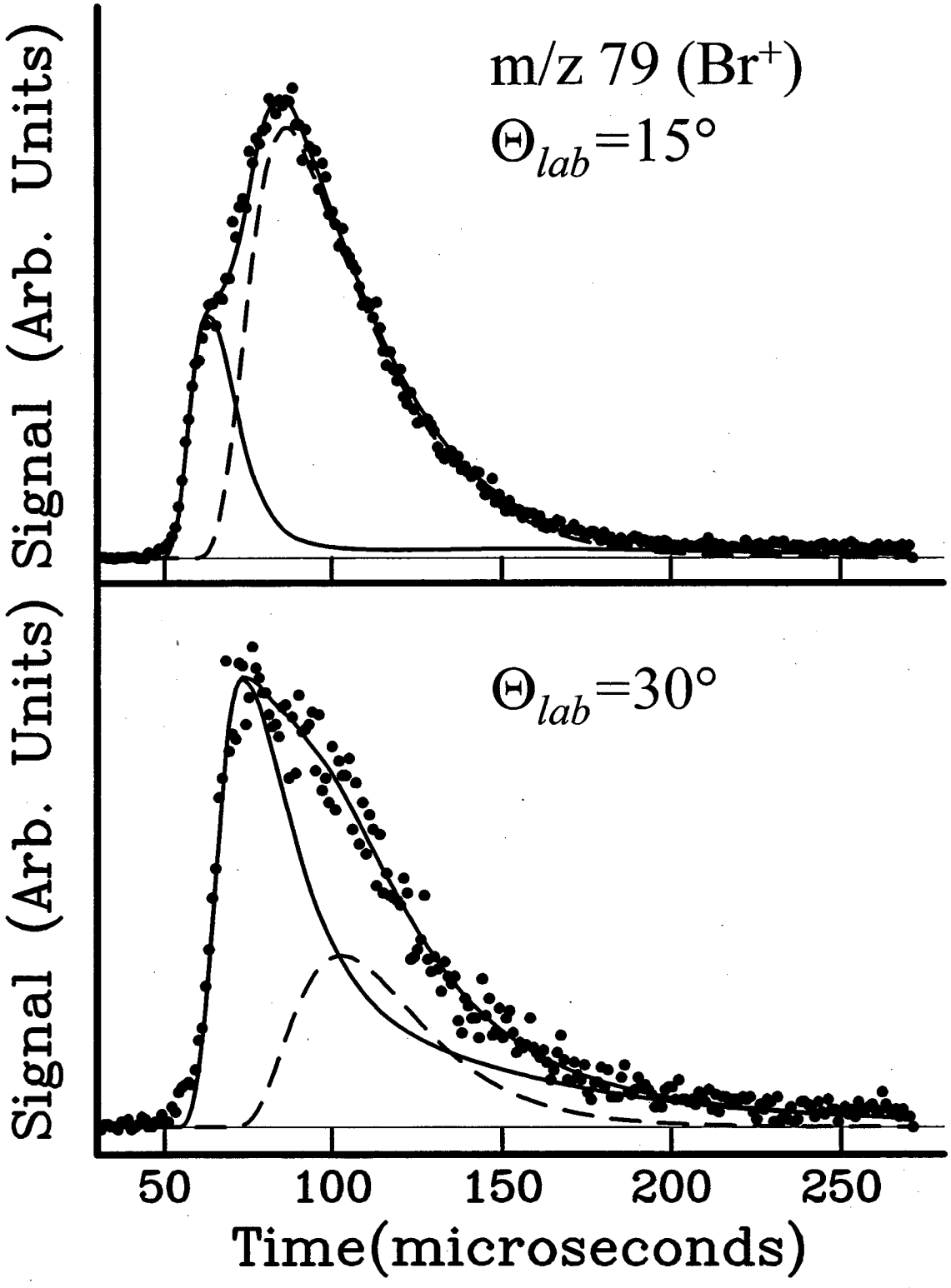
m/z 79 (Br+)
Θlab=15°
Θlab=30°
Signal (Arb. Units)
Signal (Arb. Units)
50
100
150
200
250
Time(microseconds)

Fig 3

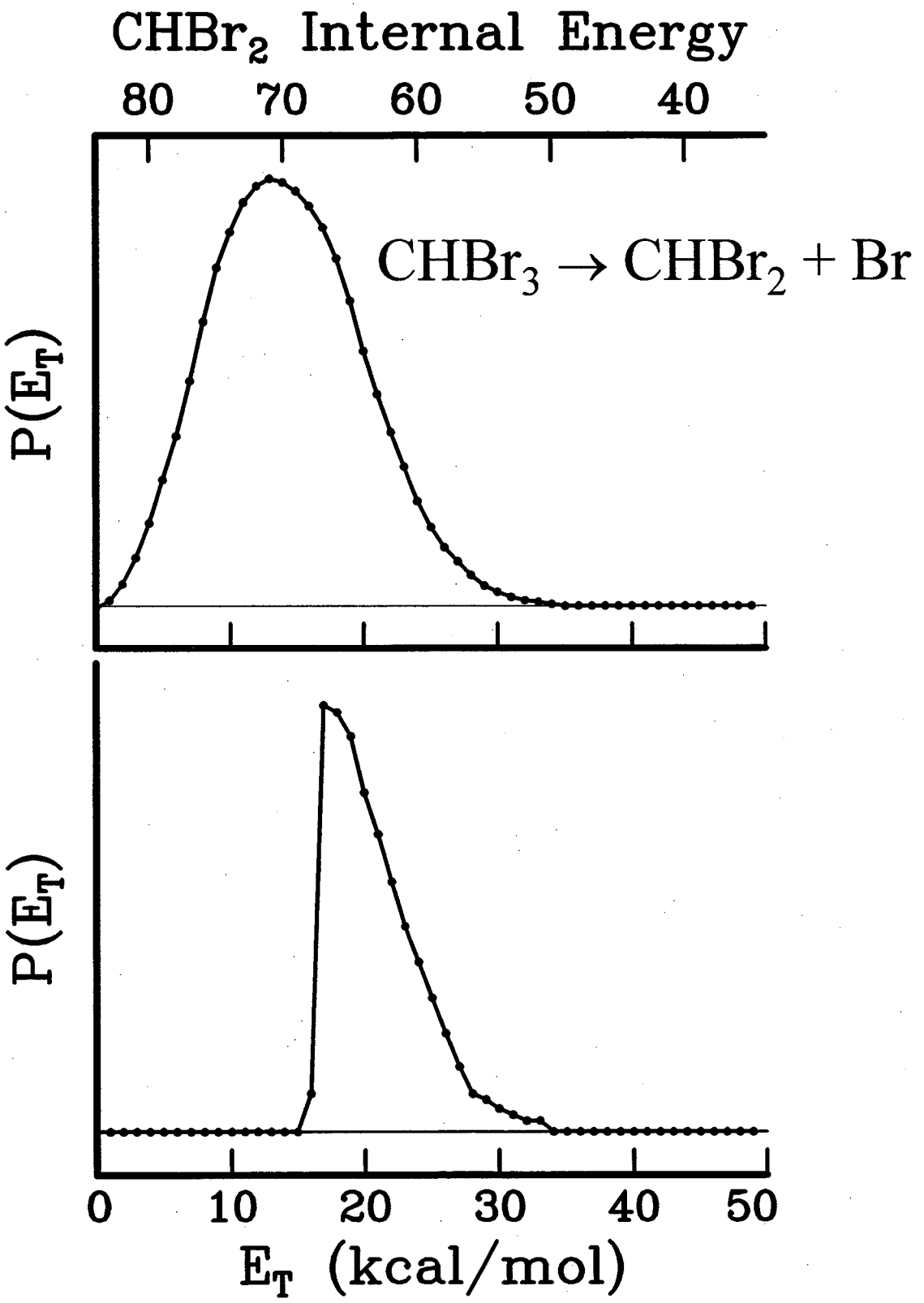
CHBr2 Internal Energy
80
70
60
50
40
CHBr3 → CHBr2 + Br
P(ET)
P(ET)
0
10
20
30
40
50
ET (kcal/mol)

Fig 4

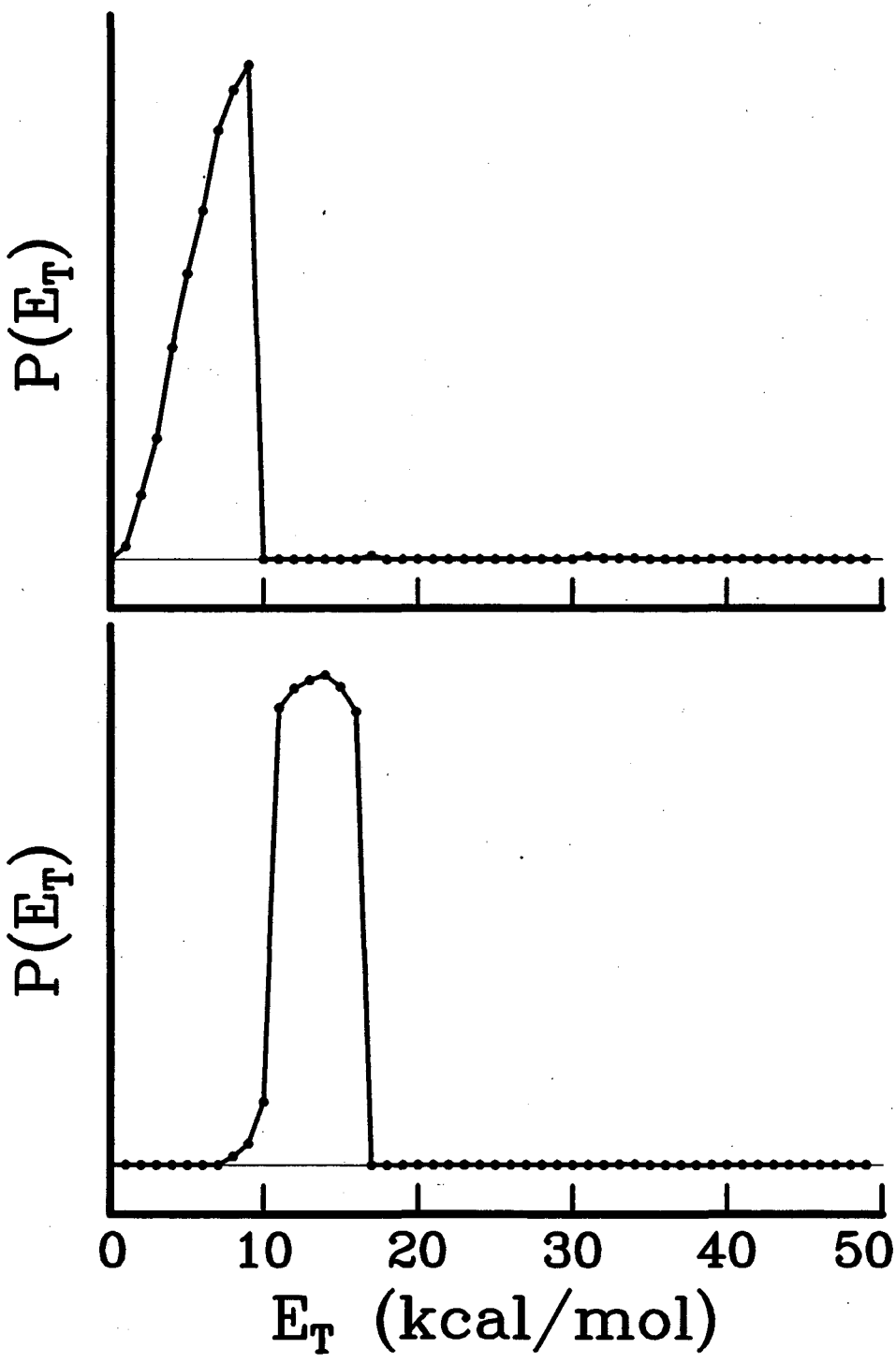

Fig 5

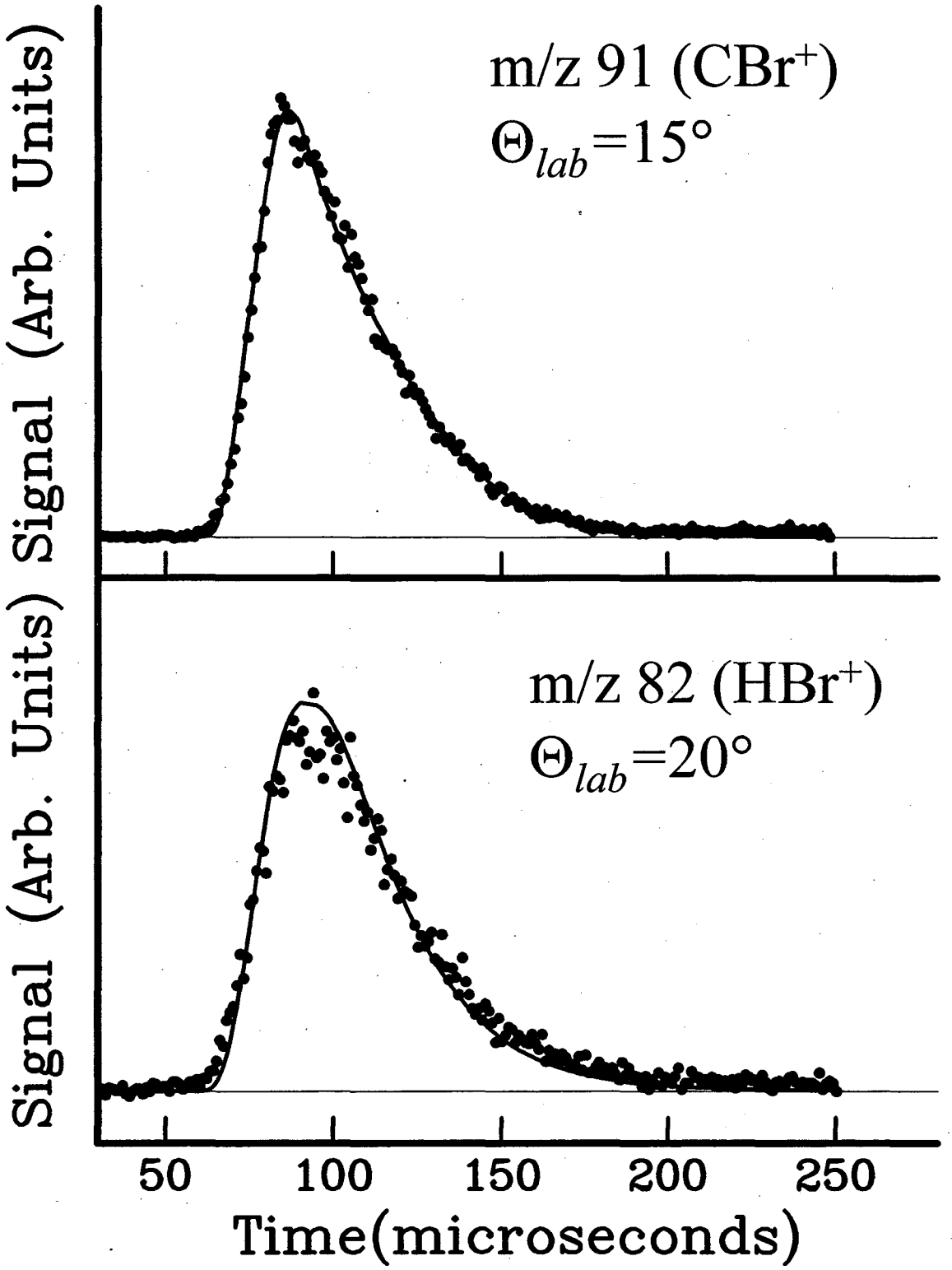
m/z 91 (CBr+)
Θlab=15°
m/z 82 (HBr+)
Θlab=20°
Signal (Arb. Units)
Signal (Arb. Units)
50
100
150
200
250
Time(microseconds)

Fig 6

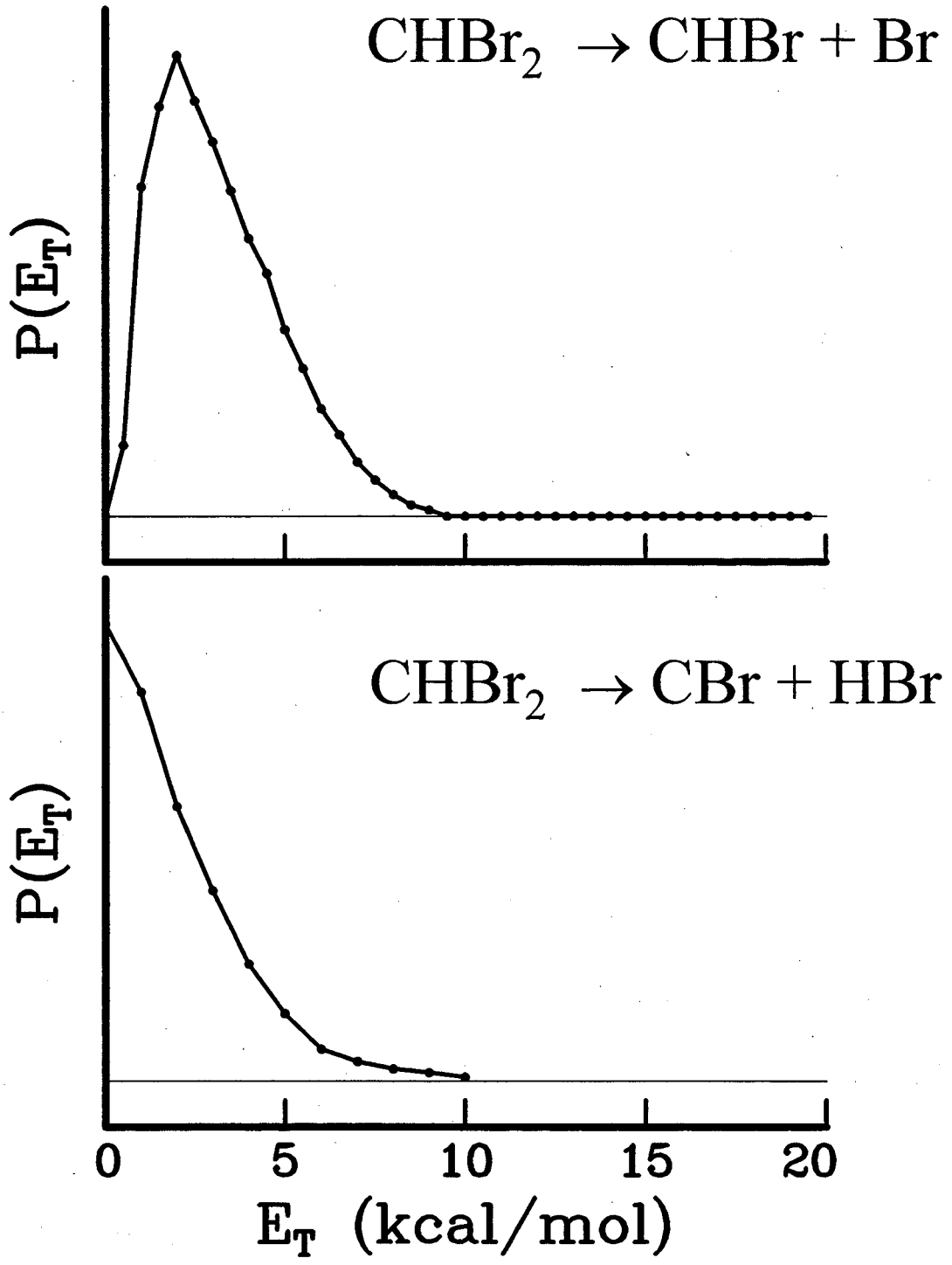

Fig 7

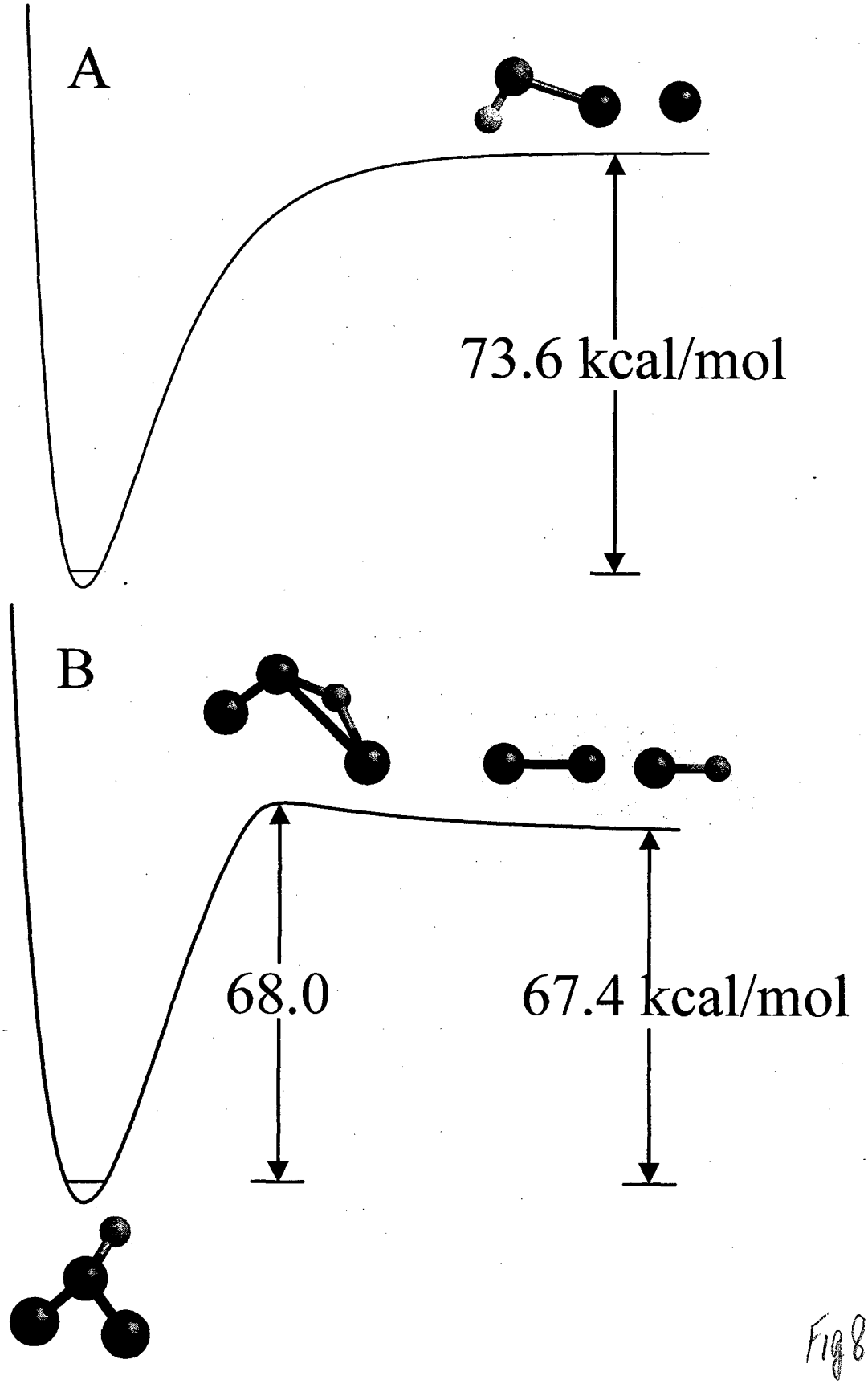

Fig 8

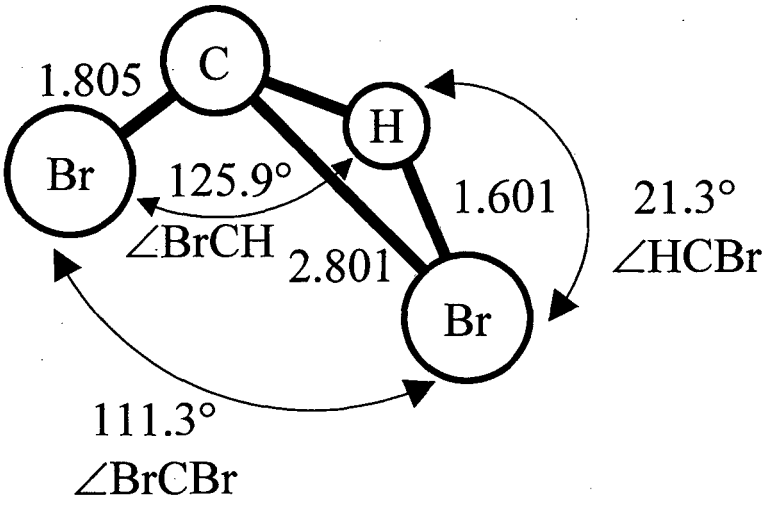
1.805
C
H
Br
125.9°
∠BrCH
1.601
21.3°
∠HCBr
2.801
Br
111.3°
∠BrCBr

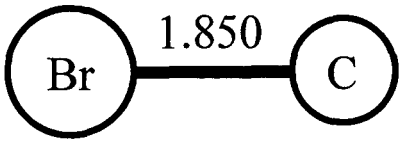
Br
1.850
C

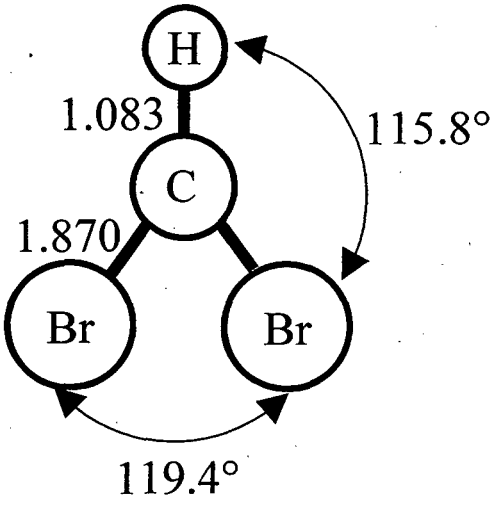
H
1.083
115.8°
C
1.870
Br
Br
119.4°

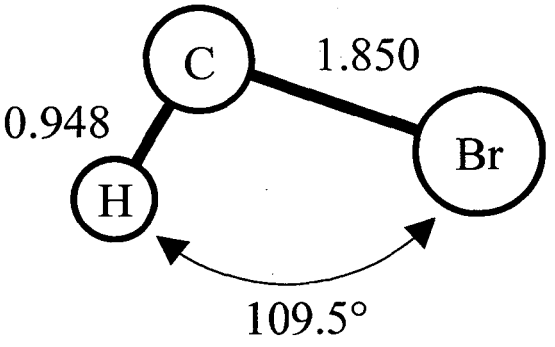
C
1.850
0.948
Br
H
109.5°

Fig 9

Ernest Orlando Lawrence Berkeley National Laboratory
One Cyclotron Road | Berkeley, California 94720

Prepared for the U.S. Department of Energy under Contract No. DE-AC03-76SF00098